



OPEN

DATA DESCRIPTOR

Multi-day dataset of forearm and wrist electromyogram for hand gesture recognition and biometrics

Ashirbad Pradhan^{1,2}, Jiayuan He^{1,3} & Ning Jiang^{1,3}

Surface electromyography (sEMG) signals have been used for advanced prosthetics control, hand-gesture recognition (HGR), and more recently as a novel biometric trait. For these sEMG-based applications, the translation from laboratory research setting to real-life scenarios suffers from two major limitations: (1) a small subject pool, and (2) single-session data recordings, both of which prevents acceptable generalization ability. **In this longitudinal database, forearm and wrist sEMG data were collected from 43 participants over three different days with long separation (Days 1, 8, and 29) while they performed static hand/wrist gestures.** The objective of this dataset is to provide a comprehensive dataset for the development of robust machine learning algorithms of sEMG, for both HGR and biometric applications. We demonstrated the high quality of the current dataset by comparing with the Ninapro dataset. And we presented its usability for both HGR and biometric applications. Among other applications, the dataset can also be used for developing electrode-shift invariant generalized models, which can further bolster the development of wristband and forearm-bracelet sensors.

Background & Summary

Recent advances in machine learning techniques have enabled applications of hand gesture recognition (HGR) using surface electromyographic (sEMG) signals. **This has further boosted the development of advanced prosthesis control systems for rehabilitation of upper limb amputees¹, and recent industrial applications have emerged using HGR for human-machine interactions in industrial² and consumer applications scenarios^{3,4}.** For these applications, the sEMG signals features are extracted and used as inputs for various machine learning techniques such as linear discriminant analysis (LDA)⁵, support vector machines (SVM)⁶ etc. for detecting hand gestures. More recently, advanced techniques such as deep neural networks (DNN) have achieved highly accurate classification performance even with simple architectures^{7,8}.

However, extensive investigation has demonstrated sEMG-based HGR has poor cross-user transference performance⁹, suggesting a calibration-free and one-size-fits-all model for all users is still elusive, which suggests that sEMG signals inherently contains individual differences, *i.e.*, biometric information. This has provided motivation for investigating the potential of sEMG as a biometric trait. Combined with the HGR property, it enables the user to set user-defined gestures as a password for enhanced security, which is not possible with other bio-signals such as electroencephalogram (EEG) and electrocardiograph (ECG). Our recent studies have provided a framework for the fusion of these codes and to facilitate such a dual-mode (password and biometrics) authentication system¹⁰.

Although, high performance of both HGR and biometric models has been previously reported, there always exists a gap between the real-world conditions and the laboratory settings, under which most of the current HGR and biometric research have been conducted conditions. It has been established in the literature, that in a multi-session protocol spreading across days, non-stationary factors including electrode shifts, skin and physical conditions will seriously affect the performance of an sEMG processing system¹¹. As there are numerous such factors, experimentally controlling each of them would increase the number of trial repetitions exponentially

¹National Clinical Research Center for Geriatrics, West China Hospital Sichuan University, Chengdu, Sichuan Province, China. ²Department of Systems Design Engineering, Faculty of Engineering, University of Waterloo, Waterloo, Canada. ³Med-X Center for Manufacturing, Sichuan University, Chengdu, Sichuan, People's Republic of China. ✉e-mail: jiangning21@wchscu.cn

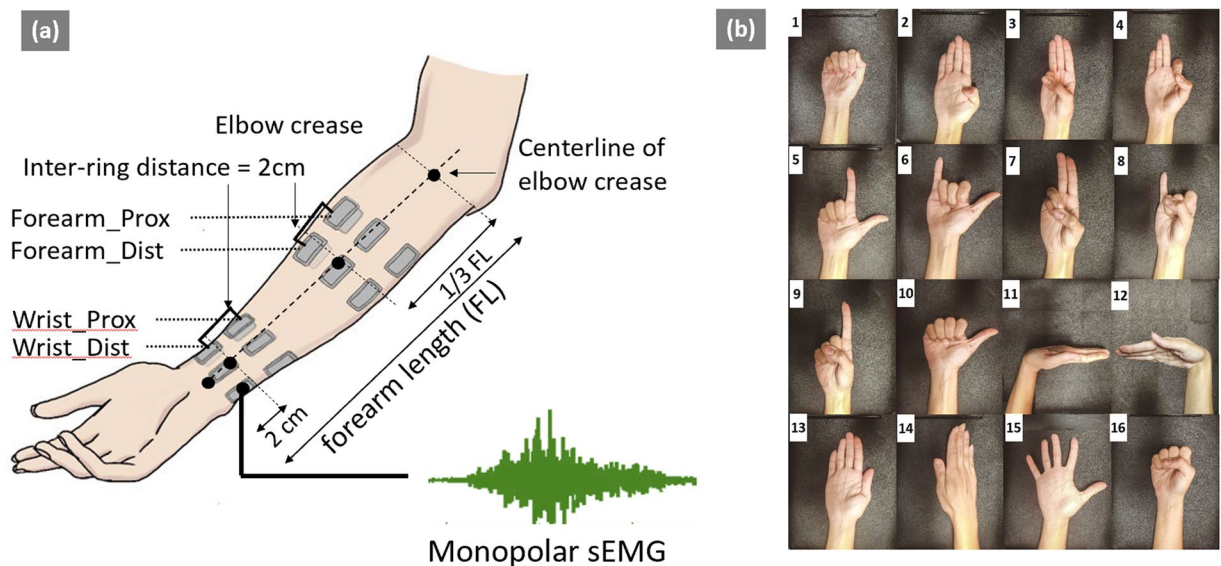


Fig. 1 Electrode Positions and Gesture List. (a) (left) shows the electrode positions used in the study. There are two groups of electrodes: forearm and wrist. Each group comprises of two rings (proximal and distal). Monopolar sEMG was recorded from a total of 28 channels (16 Forearm and 12 wrist). (b) (right) shows the Sixteen gesture classes investigated in the study (numbered 1–16): lateral prehension (LP), thumb adduction (TA), thumb and little finger opposition (TLFO), thumb and index finger opposition (TIFO), thumb and little finger extension (TLFE), thumb and index finger extension (TIFE), index and middle finger extension (IMFE), little finger extension (LFE), index finger extension (IFE), thumb extension (TE), wrist flexion (WF), wrist extension (WE), forearm supination (FS), forearm pronation (FP), hand open (HO), and hand close (HC). The REST gesture was also collected in each trial repetition.

and hence can be arduous. Nevertheless, a multi-day dataset with a sufficiently large subject pool is warranted for validating the effectiveness of sEMG applications such as HGR and biometrics.

Some open-access databases of multi-day sEMG recordings of forearm muscles are publicly available^{12–16}. Two databases with large subject pool (>40) involved two days of data collection^{14,15}. While one of them has as low as six channels¹⁵, some others utilized a high-density (HD) sEMG setup^{12,13,16}. Only three studies involved more than two of data collection days, but the number of subjects was smaller (<11)^{12,17,18}. Only one study with three days of data recording, had a sample size of 20 subject, with only signals from the forearm¹⁹. To explore the robustness and accuracy of HGR and biometrics, it is imperative to have a database with larger subject pool sizes, recorded across multiple days and comprising numerous gestures.

In the current study, we present an open-access named Gesture Recognition and Biometrics electroMyogram (GrabMyo) Dataset^{20,21}. GrabMyo consists of 43 participants (subsequently termed as users), three sessions in three separate days (subsequently termed as sessions) of data collection, 16 hand and finger gestures each with seven repetitions (subsequently termed as trials). To our best knowledge, the presented dataset is the largest sEMG dataset in terms of the total number of recording sessions (43 users \times 3 days = 129 recording sessions). A unique feature of GrabMyo is that the sEMG signals were recorded from both forearm and wrist positions. A graphical representation of electrode positions and the list of gestures investigated in the study is shown in Fig. 1a,b. The sampling frequency of the recorded signals was selected as 2048 Hz. To obtain generalizable data, special effort was taken such as 1) electrode positioning protocol for each session, 2) normal level force instruction, 3) rest duration for avoiding fatigue, 4) un-uniform interval between data collection sessions (Days 1, 8, and 29) and 5) data collection from healthy users (subjects with a single session of sickness have been eliminated from the study). These considerations are explained in greater detail in the Methods section. The dataset provides a valuable resource for sEMG-based HGR and biometrics research, particularly for improving algorithms' robustness in a multi-day scenario and cross-user generalization ability.

Methods

Subjects and ethical requirements. We recruited 43 healthy participants (23 M, 20 F) for the study spanning three different days: day 1, day 8 and day 29. The participants were students and staffs from the University of Waterloo. The average age was 26.35 ± 2.89 , and the average forearm length (measured from the styloid process on the wrist to the olecranon on the elbow) was 25.15 ± 1.74 cm. More details about the dataset and the participant characteristics are reported in Table 1. Individuals with any existing muscle pain, skin allergies, and those who were unable to complete the three sessions due to any unprecedented circumstances were excluded from the study. For the third session (day 29), a range of 3 days was provided for some participants who couldn't make it to the specific appointment. Before the enrolment, the participants were provided an oral and written explanation of the procedures and signed an informed consent form. They were informed that they could withdraw from

Participant Characteristics	Values
# Males (# Females)	23 (20)
# Right-handed (#Left)	38 (5)
Age (years)	26.35 \pm 2.89
Forearm length (cm)	25.15 \pm 1.74
Forearm circumference (cm)	24.10 \pm 2.27
Wrist circumference (cm)	16.18 \pm 1.21

Table 1. Database Summary. The forearm length is measured from the olecranon process to the ulnar styloid. The forearm circumference is measured at a distance one-third from the elbow joint. The wrist circumference is measured 2 cms away from the ulnar styloid process.

the study at any point. The experiments were conducted following the Declaration of Helsinki and the research protocol was approved by the Office of Research Ethics of the University of Waterloo (ORE# 31346).

Acquisition setup. The experimental setup consisted of a PC and a monitor mounted on a desk, 0.75 m in front of a height-adjustable chair. The EMGUSB2+ (OT Bioelettronica, Italy), a commercial amplifier, was used for acquiring the sEMG signals. The gain of the device was set to 500, and the sampling rate was set to 2048 Hz. Pre-gelled skin-adhesive monopolar sEMG electrodes (AM-N00S/E, Ambu, Denmark) were used.

Prior to the experiment, the user's forearm length is measured as the distance between the olecranon process and the ulnar styloid process. The forearm circumference is measured at one-third of the forearm length from the olecranon process. The wrist circumference is measured at 2 cm away from the ulnar styloid process. Prior to electrode placement, the skin surface was shaved to remove hairs, cleaned with an alcohol swab, and abraded with a paper towel. For the forearm electrode placement, sixteen sEMG electrodes were placed in the form of two rings, each consisting of eight electrodes equally spaced around the forearm, forming eight bipolar pairs. The center-to-center distance between the two forearm-rings was maintained at 2 cm. For the wrist electrode setup, twelve monopolar sEMG electrodes of the same type as the forearm rings were placed in the form of two rings, each consisting of six electrodes equally spaced around the wrist and forming six bipolar pairs. The center-to-center distance between the two wrist-rings was maintained at 2 cms, the same as the forearm setup. Therefore, a total of 28 monopolar sEMG electrodes were used for each session, which forms four electrode rings: proximal and distal rings for the forearm and wrist. A detailed pictorial representation is provided in Fig. 1a. To maintain consistency of the positions of the electrodes across all participants, the first electrode in each ring (total rings = 4) was anatomically positioned on the center-line of the elbow crease as shown in Fig. 1a^{22,23}. Although a standardized electrode placement protocol was followed for each session, no marks were left on the participant's skin. This intentionally induced uncertainty in the exact electrode positions corresponds to the real-life scenario where it is not realistic, if possible at all, to place an electrode band at the same position across multiple sessions.

Acquisition protocol. For each experimental session, following the acquisition setup, the participant is seated comfortably on the chair with both their upper limbs in a resting position. Visual instructions for performing the gestures were provided on the computer screen placed in front of the participants. The participants were instructed to perform the gestures at a normal force level, or similar to how they would normally do it during daily activities. For an estimate of "normal force", the participants were asked to perform multiple trial contractions at three self-defined force levels: soft, hard and medium contractions, where a medium level corresponds to the contraction of the normal force. The following 16 hand and wrist gestures were included in the current study (presented in Fig. 1b): Lateral prehension (LP), thumb adduction (TA), thumb and little finger opposition (TLFO), thumb and index finger opposition (TIFO), thumb and little finger extension (TLFE), thumb and index finger extension (TIFE), index and middle finger extension (IMFE), little finger extension (LFE), index finger extension (IFE), thumb extension (TE), wrist flexion (WF), wrist extension (WE), forearm supination (FS), forearm pronation (FP), hand open (HO), and hand close (HC). The order of the 16 gestures was randomized and a resting (REST) trial was collected after all 16 gestures were performed once. A ten-seconds relaxing period was provided between each trial. One continuous data acquisition of 17 gestures (including the REST) is called one run. First, a trial run was performed to ensure that the participants understood the experimental protocol. Following the trial run, seven runs were recorded for each user, resulting in 119 contractions (17 \times 7). Any accidental gesture or no-activity/delayed-activity was noted and the respective gesture's replacement contraction were performed after each run. The user could also request additional rest when he/she felt necessary. The entire session was repeated on day 8 (after 1 week) and day 29 (after 1 month).

Signal processing. The sEMG signals were bandpass filtered between 10 Hz and 500 Hz using a fourth-order Butterworth filter. A notch filter of 60 Hz was employed to remove the powerline noise that might have affected the signal recording.

Repository	Folders	Sub-Folders	Files	Description
PhysioNet	Session 1	session <i>i</i> _subject <i>j</i>	session <i>i</i> _subject <i>j</i> _gesture <i>k</i> _trial <i>l</i> .dat	<i>i</i> ∈ [1,2,3] represents the session(day) index
	Session 2		session <i>i</i> _subject <i>j</i> _gesture <i>k</i> _trial <i>l</i> .hea (.dat file contains 10240 × 32 hexadecimal values.	<i>j</i> ∈ [1, 2,...43] represents the subject index
	Session 3		.hea file contains signal information such as sampling frequency, units and gain)	<i>k</i> ∈ [1, 2,...17] represents the gesture index <i>l</i> ∈ [1, 2,...7] represents the trial index
IEEE Dataport	Session 1	subject <i>i</i> _session <i>j</i>	session <i>i</i> _subject <i>j</i> .mat (.mat file contains 17 × 7 cell matrix. each cell contains 10240 × 32 numeric array)	<i>i</i> ∈ [1, 2, 3] represents the session(day) index
	Session 2			<i>j</i> ∈ [1, 2,...43] represents the subject index
	Session 3			
Additional Files				
PhysioNet	<N/A>	<N/A>	readme.txt, Subject-info.csv, MotionSequence.txt, GestureList.jpg, DeviceInfo.pdf, ElectrodeLocation.pdf	readme.txt general information of the dataset and reading data files.
				MotionSequence.txt provides gesture definitions and their sequence
				GestureList.jpg provides pictorial representation of hand gestures.
IEEE Dataport	<N/A>	<N/A>	Subject-info.csv, MotionSequence.txt, GestureList.jpg	DeviceInfo.pdf describes the configuration of acquisition device.
				ElectrodeLocation.pdf illustrates the positioning of electrode sensors.
				Subject-info.csv contains participant anthropometric information

Table 2. Multi-Day EMG Database. MATLAB Codes: File Reading and Signal Processing (explained in Code availability section). For the physionet.org repository, the signal files are converted to the waveform database (WFDB) format (a *.dat file containing the signed 16 bit quantized value and *.hea file with the same name containing the scaling factors. For the IEEE Dataport *.mat file with same name is generated which consists of multiple recordings from trials and gestures.

Data Records

Data records^{20,21} presented in this section and accompanying description files are available online in PhysioNet (<https://physionet.org/about/database/>) and IEEE Dataport (<https://ieee-dataport.org/datasets>). The database consists of 43 participants, three sessions in three separate days (subsequently termed as sessions) of data collection, and 17 gestures (including REST) each with seven repetitions. All the sEMG recordings are 5 seconds in duration, collected from 28 channels (16 forearm and 12 wrist), and sampled at 2048 Hz.

The components of the released repositories are described in detail (Table 2) and are organized as follows: waveform data and additional files.

Waveform data. For the PhysioNet Database, the sEMG recordings are provided in the waveform database (WFDB) format, which is considered the most widely used medium for storing physiological signals and waveform data²⁴. There exist numerous open-source WFDB libraries for commonly used analysis tools using MATLAB and Python. The WFDB allows a structured way of storing the sEMG recording in the form of a tuple of two files: a dat-file containing the binary raw data and a corresponding header file with the same name and a hea-extension. The hea-extension contains all the signal-specific metadata such as the channel names, sampling frequency, and the scaling factor for converting the signal to physical units (in mVs).

For the IEEE database, the signal files are saved as .mat files. The mat file extension allows users a convenient approach for obtaining the sEMG recordings in the physical unit format (additional conversion is not necessary). Additionally, the mat files allow data to be organized as cells where multiple gestures and repetitions from a single session can be presented together.

Additional files. The additional files provide supplementary information such as the participant anthropometrics, electrode positioning guidelines, device configuration, the sequence of gestures, and their descriptions. MATLAB codes are also provided for reading the data files and subsequent feature extraction as explained in the Code Availability section.

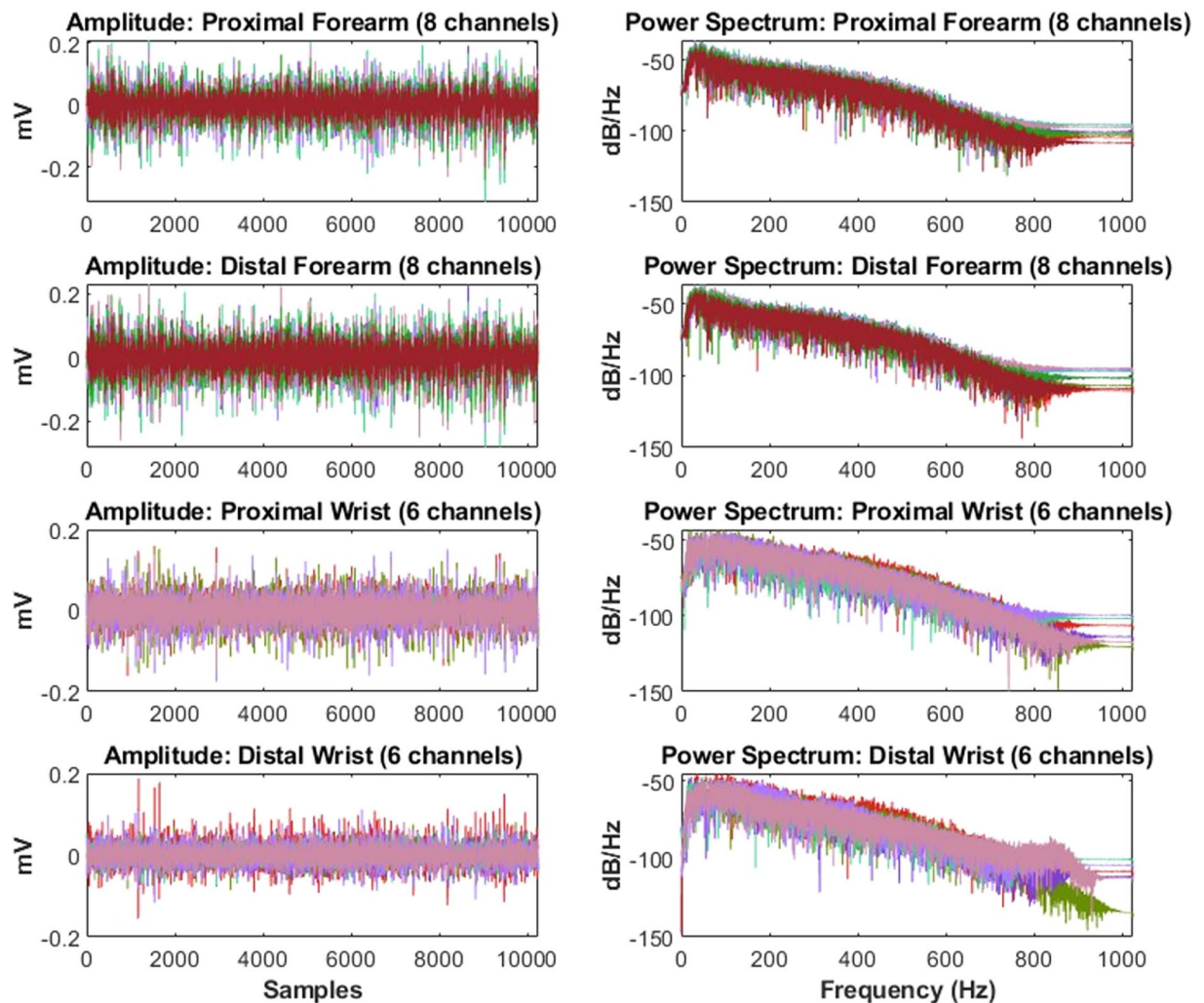


Fig. 2 Representative amplitude and power spectrum plots. Left Column: The amplitude values (in mV) for the four electrode rings: proximal and distal forearm and wrist (from top to bottom). Right Column: The fast fourier transform (FFT) power spectrum (in dB/Hz) for the four electrode rings: proximal and distal forearm and wrist (from top to bottom). The forearm rings constitute 8 channels each and the wrist rings constitute 6 channels each (shown in different colors).

Technical Validation

A specific trial of an individual user case was chosen at random and the amplitude and frequency components were analyzed as shown in Fig. 2. It was observed that all 28 channels of forearm and wrist possessed equal amplitude and power spectrum distribution. In the following sections, signal processing techniques are discussed for analysis and technical validation of the sEMG signals. As well, the original references where the methods were described in depth are provided. For comparison, the validation results are provided along with those for the widely used Ninapro DB2: Exercise B comprising 40 users and 17 gestures.

Signal-to-noise ratio (SNR). The spectral properties of each sEMG signal recording were analysed and the SNR (in dB) was measured as the ratio between the power of the signal to the power of the noise^{25,26}. As the types of the artifacts were unknown in our case, the power of the noise was estimated as the power of sEMG recordings during the rest trial. The average SNR of all the signals (14.565 ± 6.385 dB) was in range with the SNR values suggested for the wrist and forearm²⁵ and they are consistently higher than those from the Ninapro database (8.001 ± 4.051 dB) (see Fig. 3a).

Correlation coefficient of Normality (CCN). The CCN was measured to analyze the amplitude distribution. For a static contraction with moderate force, the sEMG can be modeled as a filtered, random, white Gaussian noise process²⁷. It has been suggested that a test of normality can provide a measure of biosignal quality, where a signal amplitude with a non-normal distribution would be considered contaminated. A Gaussian distribution with equal mean and variance to that of the recording is generated²⁸. The CCN is defined as the Pearson correlation coefficient between the histogram bin values of the sEMG recording and the normal density function value for the corresponding bins. A value close to 1 is considered a normal distribution. It was observed that the CCN of

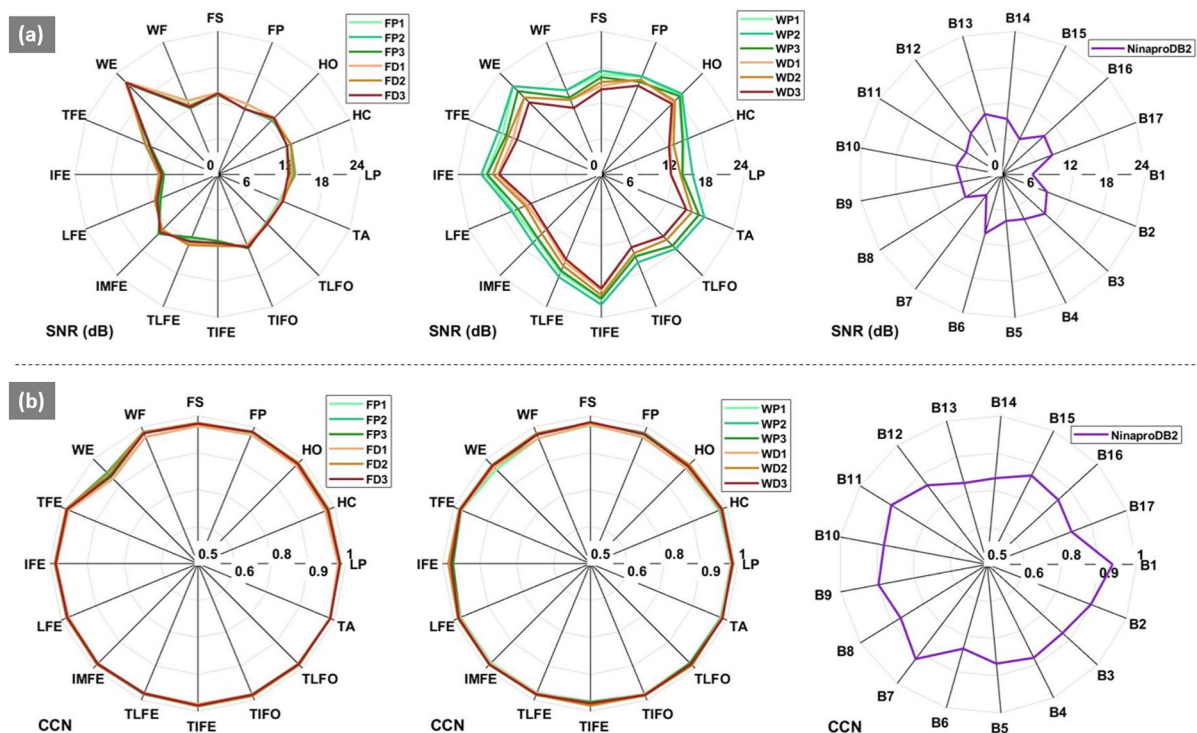


Fig. 3 SNR and CCN comparison plots. Panel **a**, *i.e.* the top row shows SNR values (dB), with each spoke representing one motion. Left: the forearm proximal and distal electrode setup for session 1–3 (added as suffix FP1, FP2,...,FD3); middle: wrist proximal and distal electrode setup for session 1–3 (added as suffix WP1,WP2,...,WD3); and (right) the Ninapro signals collected from the forearm for a single day. Panel **b**, *i.e.* the bottom row shows the CCN values for the forearm (left), wrist (middle) and Ninapro data (right) in a similar manner.

all the signals (0.975 ± 0.041) was close to 1 which was consistently higher than those from the Ninapro database (0.848 ± 0.075) (see Fig. 3b).

Standard HGR and biometric analysis. Prior to HGR and Biometric evaluation, the signals were first processed and then features were extracted as described below. The forearm rings (eight channels) and the wrist rings (six channels), the monopolar sEMG signals were first re-referenced by a common average procedure. The processed signals were then segmented into 200 ms-width windows, with a 150 ms overlap. Each window was then processed using Hudgins's time-domain (TD) feature extraction²⁹. Time-domain features (mean absolute value, zero crossing, slope sign changes, and waveform length) were extracted from filtered data²². Therefore, for a forearm setup, the feature vector consisted of $8 \times 4 = 32$ features, while the wrist setup consisted of $6 \times 4 = 24$ features.

For the biometric analysis, a matching score, commonly the Mahalanobis distance, is used to assess if it's a match (access granted) or no match (access denied)^{10,22,23}. To maintain consistency in the HGR and biometric analyses, a Mahalanobis distance classifier was implemented for both analyses. For a given feature vector sample p (the input), its Mahalanobis distance $S_{i,j}$ with the i th gesture and the j th user, was defined as

$$S_{i,j}(p) = \sqrt{(p - \mu_{i,j})^T \Sigma_{i,j}^{-1} (p - \mu_{i,j})}, \quad (1)$$

where $\mu_{i,j}$ is the centroid of the i th gesture class and the j th user and $\Sigma_{i,j}$ is the covariance matrix for the specific gesture and user class. Both the parameters are calculated from the system training data and the sample p is from the system testing data. The leave-one-out (LOO) cross-validation scheme was used, where six trials were used for training and one trial for testing. Figure 3a,b, and Table 3 demonstrate the results of the technical validation as described in the following sections.

HGR evaluation. In this study, the HGR analysis was performed in a user-specific scheme. For a particular user and a particular gesture, the true class consisted of the feature vectors from the target gesture of the user and the false class consisted of the feature vectors from the remaining 15 gestures of that user (the rest gesture was excluded from the HGR analysis to maintain consistency with biometric analysis). Similarly, for the Ninapro database, the true class consisted of feature vectors from the target gesture of a specific user and the false class consisted of the feature vectors of the remaining 16 gestures. For the performance analysis a receiver operating characteristic (ROC), where the true positive rate (sensitivity) was plotted against the false positive rate ($1 - \text{specificity}$) by varying the threshold distance of correct gesture prediction. The true positive rate or sensitivity

Electrode Setup	HGR Evaluation (AUC)	Biometric Evaluation (EER)
Forearm	0.948 (± 0.018)	0.028 (± 0.007)
Wrist	0.941 (± 0.021)	0.038 (± 0.006)
Ninapro (Forearm)	0.875 (± 0.034)	0.038 (± 0.013)

Table 3. Mean (\pm STD) HGR and Biometric performance.

represents the probability of detecting a correct gesture, while the false positive rate is the probability of detecting an incorrect gesture. The area under the curve (AUC) is calculated from the ROC curve³⁰. The ROC curve and the AUC values for all the users, days, and gestures are averaged and reported separately for the forearm and wrist electrode positions. Figure 4a shows the ROC plots for HGR analysis. It was observed that the AUC for the forearm was 0.948 (± 0.018) and for the wrist was 0.941 (± 0.021). Both the values were comparatively higher than the corresponding AUC value of 0.875 (± 0.034) for the NinaPro data.

Biometric evaluation. In this study, the verification mode of biometrics was used to demonstrate the feasibility of multi-day sEMG-based biometrics. In this mode, the true user's identity and the corresponding gesture are known to the system. As such, for a specific user, the true class consisted of the feature vectors from the target gesture (e.g. the passcode) of that user and the false class consisted of the feature vectors of the remaining 42 users for that gesture. Similarly, for the Ninapro database, the true class consisted of feature vectors from the target gesture of a specific user and the false class consisted of the feature vectors from the remaining 39 users for that gesture. For the performance analysis a receiver operating characteristic (ROC), where the true positive rate (sensitivity) was plotted against the false positive rate (1 – specificity) by varying the threshold distance of correct biometric authentication. The true positive rate or sensitivity represents the probability of detecting a correct hand gesture, while the false positive rate is the probability of detecting an incorrect hand gesture. The equal error rate (EER), is obtained from the ROC curve, where the false positive rate is equal to the false negative rate (1 – sensitivity)³⁰. The ROC curve and the EER values for all the users, days, and gestures are averaged and reported separately for the forearm and wrist electrode positions. Figure 4b shows the ROC plots for Biometric analysis. It was observed that the EER for the forearm was 0.028 (± 0.007) and for the wrist was 0.038 (± 0.006). Both the values were comparatively lower than the corresponding EER value of 0.038 (± 0.013) for the NinaPro data.

Usage Notes

As evident from the title, the GRABMyo Dataset has two major applications: HGR using machine learning approaches and sEMG-based biometrics. The true potential of GRABMyo are three-fold: 1) large subject-pool, 2) multi-day session, and 3) both wrist and forearm channels. Through the *Signal Analysis* section, we will explain processing sEMG recordings and the cross-validation approach for obtaining reliable benchmark results using machine learning algorithms. Following this, the *Future Direction* lists novel research strategies for HGR and Biometric analysis which could be bolstered using the large multiday dataset.

Signal analysis. The MATLAB code `fileread.m` allows the users to read data files along with their signal-specific metadata. After conversion to a numeric format, the data is structured as matrixes with timepoints as rows and monopolar sEMG channels as columns. The channel names provided can be used for separate forearm and wrist electrode rings and also for forming bipolar pairs between them³¹. The processed data is then windowed, and features can be extracted using multiple techniques³². A widely used frequency division technique³³ is provided as a sample feature extraction in `feature_extraction.m`. The gesture labels are provided by `MotionSequence.txt` which allows the extracted features to be matched to the specific gestures and their respective users. For HGR and biometric applications, the output classes are the gestures and users, respectively which can be used for developing machine learning and deep learning architectures. The data provides seven trial repetitions, hence seven-fold cross-validation (six-folds for training and one-fold for testing) can be used to simulate a near-practical scenario, where the testing data is recorded separately from the training data. A more robust analysis i.e., the multi-day analysis with a 3-fold cross-validation can be employed, where subsets of data from two days are used for training and the data from the remaining day is used for testing.

Future Directions. Some future research directions are:

Improving biometric authentication. One unique advantage of the EMG biometric trait, in particular for authentication applications, is the combination of user-specific biometrics with user-defined gestures as passcodes, the latter of which is not possible with other bio-signals such as electroencephalogram (EEG) and electrocardiogram (ECG). A multi-code EMG-based biometric framework can be used to combine the gestures and improve authentication performance and security¹⁰.

Biometric identification. Another major biometric application is the identification mode where the system predicts the identity of the presenting user by finding the closest match. The identification is a more error-prone application as the system makes N comparisons, where N is the number of users. Therefore, the factors affecting system performance such as multiple days and sample size of the database need to be investigated for real-life applications.

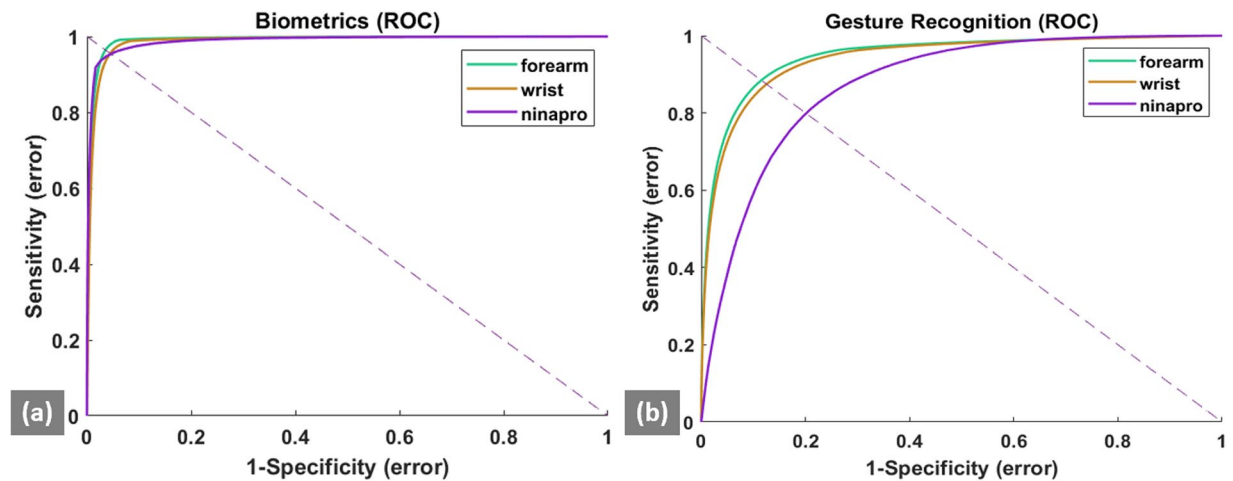


Fig. 4 ROC curves for HGR and Biometric validation. The ROC curves are plotted for the HGR evaluation (a) and Biometric Evaluation (b) for the forearm and wrist data averaged for the multiple users ($N = 43$), sessions ($N = 3$) as well as for the Ninapro Data (#users = 40, #sessions = 1). The dotted line represents the point of intersection on the ROC curve from which the EER value is obtained.

Subject independent gesture recognition. Extensive research on EMG has been performed on gesture recognition with application in rehabilitation using prosthetic and orthotic devices, home application for assisting daily activities, virtual environment control, and sign language recognition^{3,4,34}. Recent studies have suggested deep learning techniques for cross-user calibration-free which trains generalized models using the population data, and hence reduces the training burden of the user^{9,35,36}. The presented large-sample dataset can provide resources for such calibration-free models.

Electrode shift-invariant techniques. One of the significant factors affecting the cross-day sEMG performance is the shift in the electrode positions. It is impossible to fix the location of armband electrodes on the forearm and wrist for daily-wear use. These variations affect the performance of both the sEMG-based biometric and gesture recognition applications. Some techniques such as classification model adaptation^{37,38} and feature space transformation using transfer learning^{35,39,40} have been suggested to address the electrode shift variations. These techniques could be further investigated to potentially improve biometrics and HGR performance.

Code availability

The custom codes used for reading the signals of the database was created in MATLAB R2017b and is freely accessible at Physionet and IEEE Dataport^{20,21}. To implement the codes, the users will need a MATLAB License

- A readme file (`readme.txt`) with instructions about how to run the code in a 2017b or higher MATLAB version.
- A Matlab script (`fileread.m`) with a simple example about how to read WFDB files and convert them to .mat format.
- A text file (`MotionSequence.txt`) which provides the gesture sequence, and thus can be used to assign class labels to input data.
- A Matlab script (`feature_extraction.m`) allows a simple example to extract frequency features using `featiDFTI.m` and `segmentEMG.m` functions.
- A Matlab function (`featiDFTI.m`) for generating frequency division technique features from sEMG Data.
- A Matlab script (`segmentEMG.m`) for implementing windowing of sEMG Data.

Received: 29 July 2022; Accepted: 11 November 2022;

Published online: 30 November 2022

References

1. Jiang, N., Dosen, S., Muller, K.-R. & Farina, D. Myoelectric control of artificial limbs—is there a need to change focus?[In the spotlight]. *IEEE Signal Processing Magazine* **29**, 152–150 (2012).
2. Qureshi, F. & Krishnan, S. Wearable hardware design for the internet of medical things (IoMT). *Sensors* **18**, 3812 (2018).
3. Wu, J., Sun, L. & Jafari, R. A wearable system for recognizing American sign language in real-time using IMU and surface EMG sensors. *IEEE J Biomed Health Inform* **20**, 1281–1290 (2016).
4. Dwivedi, A., Kwon, Y. & Liarokapis, M. in 2020 IEEE International Conference on Systems, Man, and Cybernetics (SMC). 3296–3303 (IEEE).
5. Englehart, K. & Hudgins, B. A robust, real-time control scheme for multifunction myoelectric control. *IEEE Trans. Biomed. Eng.* **50**, 848–854 (2003).
6. Tavakoli, M., Benussi, C., Lopes, P. A., Osorio, L. B. & de Almeida, A. T. Robust hand gesture recognition with a double channel surface EMG wearable armband and SVM classifier. *Biomed. Signal Process. Control* **46**, 121–130 (2018).
7. Clarke, A. K. *et al.* Deep learning for robust decomposition of high-density surface EMG signals. *IEEE Trans. Biomed. Eng.* **68**, 526–534 (2020).

8. Chen, L., Fu, J., Wu, Y., Li, H. & Zheng, B. Hand gesture recognition using compact CNN via surface electromyography signals. *Sensors* **20**, 672 (2020).
9. Campbell, E., Phinyomark, A. & Scheme, E. Deep Cross-User Models Reduce the Training Burden in Myoelectric Control. *Front. Neurosci.* **15** (2021).
10. Pradhan, A., He, J. & Jiang, N. Score, Rank, and Decision-Level Fusion Strategies of Multicode Electromyogram-based Verification and Identification Biometrics. *IEEE J Biomed Health Inform* (2021).
11. Benatti, S., Farella, E., Gruppioni, E. & Benini, L. in *BIO SIGNALS*. 45–54.
12. Amma, C., Krings, T., Böer, J. & Schultz, T. in *Proceedings of the 33rd Annual ACM Conference on Human Factors in Computing Systems*. 929–938.
13. Chen, J., Bi, S., Zhang, G. & Cao, G. High-density surface EMG-based gesture recognition using a 3D convolutional neural network. *Sensors* **20**, 1201 (2020).
14. Kaczmarek, P., Mańkowski, T. & Tomczyński, J. putEMG—a surface electromyography hand gesture recognition dataset. *Sensors* **19**, 3548 (2019).
15. Turgunov, A., Zohirov, K. & Muhtorov, B. in *2020 IEEE 14th International Conference on Application of Information and Communication Technologies (AICT)*. 1–4 (IEEE).
16. Jiang, X. *et al.* Open Access Dataset, Toolbox and Benchmark Processing Results of High-Density Surface Electromyogram Recordings. *IEEE Trans. Neural Syst. Rehabil. Eng.* **29**, 1035–1046 (2021).
17. Giordaniello, F. *et al.* in *2017 International Conference on Rehabilitation Robotics (ICORR)*. 1148–1153 (IEEE).
18. Fang, Y., Zhang, X., Zhou, D. & Liu, H. Improve inter-day hand gesture recognition via convolutional neural network based feature fusion. *Int J HR* (2020).
19. Côté-Allard, U. *et al.* A transferable adaptive domain adversarial neural network for virtual reality augmented EMG-based gesture recognition. *IEEE Trans. Neural Syst. Rehabil. Eng.* **29**, 546–555 (2021).
20. Jiang, N., Pradhan, A. & He, J. Gesture Recognition and Biometrics ElectroMyogram (GRABMyo) (version 1.0.1). *PhysioNet*. <https://doi.org/10.13026/701k-gs64> (2022).
21. Pradhan, A., Jiang, N. & He, J. Gesture Recognition and Biometrics ElectroMyogram (GRABMyo) Dataset. *IEEE Dataport* <https://doi.org/10.21227/82v9-2b79> (2022).
22. Pradhan, A., He, J. & Jiang, N. Performance Optimization of Surface Electromyography based Biometric Sensing System for both Verification and Identification. *IEEE Sens J.* (2021).
23. He, J. & Jiang, N. Biometric From Surface Electromyogram (sEMG): Feasibility of User Verification and Identification Based on Gesture Recognition. *Front Bioeng Biotechnol* **8**, 58 (2020).
24. Goldberger, A. L. *et al.* PhysioBank, PhysioToolkit, and PhysioNet: components of a new research resource for complex physiologic signals. **101**, e215–e220 (2000).
25. Botros, F. S., Phinyomark, A. & Scheme, E. Electromyography-based gesture recognition: Is it time to change focus from the forearm to the wrist? *IEEE Trans Industr Inform* **18**, 174–184 (2020).
26. Sinderby, C., Lindstrom, L. & Grassino, A. Automatic assessment of electromyogram quality. *J. Appl. Physiol.* **79**, 1803–1815 (1995).
27. Shwedyk, E., Balasubramanian, R. & Scott, R. A nonstationary model for the electromyogram. *IEEE Trans. Biomed. Eng.*, 417–424 (1977).
28. Fraser, G. D., Chan, A. D., Green, J. R. & MacIsaac, D. T. in *2013 IEEE International Symposium on Medical Measurements and Applications (MeMeA)*. 196–200 (IEEE).
29. Hudgins, B., Parker, P. & Scott, R. N. A new strategy for multifunction myoelectric control. *IEEE Trans. Biomed. Eng.* **40**, 82–94 (1993).
30. Bolle, R. M., Connell, J. H., Pankanti, S., Rath, N. K. & Senior, A. W. *Guide to biometrics*. (Springer Science & Business Media 2013).
31. Staudenmann, D., Kingma, I., Stegeman, D. F. & van Dieën, J. H. Towards optimal multi-channel EMG electrode configurations in muscle force estimation: a high density EMG study. *J. Electromyogr. Kinesiol.* **15**, 1–11 (2005).
32. Phinyomark, A., N. Khushaba, R. & Scheme, E. Feature extraction and selection for myoelectric control based on wearable EMG sensors. *Sensors* **18**, 1615 (2018).
33. Pradhan, A., Jiang, N., Chester, V. & Kuruganti, U. Linear regression with frequency division technique for robust simultaneous and proportional myoelectric control during medium and high contraction-level variation. *Biomed. Signal Process. Control* **61**, 101984 (2020).
34. Castellini, C. & Van Der Smagt, P. Surface EMG in advanced hand prosthetics. *Biol. Cybern.* **100**, 35–47 (2009).
35. Côté-Allard, U. *et al.* Unsupervised domain adversarial self-calibration for electromyography-based gesture recognition. *IEEE Access* **8**, 177941–177955 (2020).
36. Côté-Allard, U. *et al.* Interpreting deep learning features for myoelectric control: A comparison with handcrafted features. *Front Bioeng Biotechnol* **8**, 158 (2020).
37. Vidovic, M. M.-C. *et al.* Improving the robustness of myoelectric pattern recognition for upper limb prostheses by covariate shift adaptation. *IEEE Trans. Neural Syst. Rehabil. Eng.* **24**, 961–970 (2015).
38. Kanoga, S. & Kanemura, A. in *2018 IEEE International Conference on Industrial Technology (ICIT)*. 1478–1483 (IEEE).
39. Paaßen, B., Schulz, A., Hahne, J. & Hammer, B. Expectation maximization transfer learning and its application for bionic hand prostheses. *Neurocomputing* **298**, 122–133 (2018).
40. Prahm, C. *et al.* Counteracting electrode shifts in upper-limb prosthesis control via transfer learning. *IEEE Trans. Neural Syst. Rehabil. Eng.* **27**, 956–962 (2019).

Acknowledgements

The authors like to thank all the participants for their valuable contribution to the development of the dataset. This work was supported by the Natural Sciences and Engineering Research Council of Canada (Discovery Grant: 072169).

Author contributions

A.P., J.H. and N.J. conceived and designed the experimental protocol and conducted the experiments. A.P. and J.H. aided in the analysis of the data and interpretation of results. A.P., J.H. and N.J. organized the database. A.P. prepared the scripts in MATLAB for sharing with the database. A.P. and N.J. wrote the manuscript, and all authors contributed to revising it.

Competing interests

The authors declare no competing interests.

Additional information

Correspondence and requests for materials should be addressed to N.J.

Reprints and permissions information is available at www.nature.com/reprints.

Publisher's note Springer Nature remains neutral with regard to jurisdictional claims in published maps and institutional affiliations.



Open Access This article is licensed under a Creative Commons Attribution 4.0 International License, which permits use, sharing, adaptation, distribution and reproduction in any medium or format, as long as you give appropriate credit to the original author(s) and the source, provide a link to the Creative Commons license, and indicate if changes were made. The images or other third party material in this article are included in the article's Creative Commons license, unless indicated otherwise in a credit line to the material. If material is not included in the article's Creative Commons license and your intended use is not permitted by statutory regulation or exceeds the permitted use, you will need to obtain permission directly from the copyright holder. To view a copy of this license, visit <http://creativecommons.org/licenses/by/4.0/>.

© The Author(s) 2022

Terms and Conditions

Springer Nature journal content, brought to you courtesy of Springer Nature Customer Service Center GmbH (“Springer Nature”).

Springer Nature supports a reasonable amount of sharing of research papers by authors, subscribers and authorised users (“Users”), for small-scale personal, non-commercial use provided that all copyright, trade and service marks and other proprietary notices are maintained. By accessing, sharing, receiving or otherwise using the Springer Nature journal content you agree to these terms of use (“Terms”). For these purposes, Springer Nature considers academic use (by researchers and students) to be non-commercial.

These Terms are supplementary and will apply in addition to any applicable website terms and conditions, a relevant site licence or a personal subscription. These Terms will prevail over any conflict or ambiguity with regards to the relevant terms, a site licence or a personal subscription (to the extent of the conflict or ambiguity only). For Creative Commons-licensed articles, the terms of the Creative Commons license used will apply.

We collect and use personal data to provide access to the Springer Nature journal content. We may also use these personal data internally within ResearchGate and Springer Nature and as agreed share it, in an anonymised way, for purposes of tracking, analysis and reporting. We will not otherwise disclose your personal data outside the ResearchGate or the Springer Nature group of companies unless we have your permission as detailed in the Privacy Policy.

While Users may use the Springer Nature journal content for small scale, personal non-commercial use, it is important to note that Users may not:

1. use such content for the purpose of providing other users with access on a regular or large scale basis or as a means to circumvent access control;
2. use such content where to do so would be considered a criminal or statutory offence in any jurisdiction, or gives rise to civil liability, or is otherwise unlawful;
3. falsely or misleadingly imply or suggest endorsement, approval, sponsorship, or association unless explicitly agreed to by Springer Nature in writing;
4. use bots or other automated methods to access the content or redirect messages
5. override any security feature or exclusionary protocol; or
6. share the content in order to create substitute for Springer Nature products or services or a systematic database of Springer Nature journal content.

In line with the restriction against commercial use, Springer Nature does not permit the creation of a product or service that creates revenue, royalties, rent or income from our content or its inclusion as part of a paid for service or for other commercial gain. Springer Nature journal content cannot be used for inter-library loans and librarians may not upload Springer Nature journal content on a large scale into their, or any other, institutional repository.

These terms of use are reviewed regularly and may be amended at any time. Springer Nature is not obligated to publish any information or content on this website and may remove it or features or functionality at our sole discretion, at any time with or without notice. Springer Nature may revoke this licence to you at any time and remove access to any copies of the Springer Nature journal content which have been saved.

To the fullest extent permitted by law, Springer Nature makes no warranties, representations or guarantees to Users, either express or implied with respect to the Springer nature journal content and all parties disclaim and waive any implied warranties or warranties imposed by law, including merchantability or fitness for any particular purpose.

Please note that these rights do not automatically extend to content, data or other material published by Springer Nature that may be licensed from third parties.

If you would like to use or distribute our Springer Nature journal content to a wider audience or on a regular basis or in any other manner not expressly permitted by these Terms, please contact Springer Nature at

onlineservice@springernature.com